INSTITUTE OF PHYSICS PUBLISHING PLASMA SOURCES SCIENCE AND TECHNOLOGY

Plasma Sources Sci. Technol. **12** (2003) S8–S15 PII: S0963-0252(03)60689-4

Electron and metastable kinetics in the nitrogen afterglow

V Guerra[1], P A Sá[2] and J Loureiro[1]

[1] Centro de Física dos Plasmas, Instituto Superior Técnico, 1049-001 Lisboa, Portugal
[2] Departamento de Física, Faculdade de Engenharia, Universidade do Porto, 4200-465 Porto, Portugal

E-mail: vguerra@theta.ist.utl.pt

Received 9 October 2002, in final form 27 January 2003
Published 18 September 2003
Online at stacks.iop.org/PSST/12/S8

Abstract

This work presents a theoretical study of the time-relaxation of both the electron energy distribution function and the populations of the different species of interest in the nitrogen afterglow of a $\omega/2\pi = 433$ MHz discharge at $p = 3.3$ Torr, in a tube with radius $R = 1.9$ cm. It is shown that collisions of highly excited $N_2(X\,^1\Sigma_g^+, v \gtrsim 35)$ molecules with $N(^4S)$ atoms may be in the origin of the observed pronounced maxima for the concentrations of various species, including electrons, occurring downstream from the discharge after a dark zone. Slow electrons remain for very long times in the post-discharge (at least up to $t \sim 10^{-3}$–10^{-2} s), and the strong coupling between the electron and metastable kinetics is clearly pointed out.

1. Introduction

The study of N_2 flowing post-discharges is currently receiving much attention, both experimental and theoretical, due to its importance in applications related to surface treatments and plasma sources of atoms [1, 2]. In order to characterize the complex phenomena occurring in the short-lived afterglow, a systematic spectroscopy observation of the most intense bands of N_2 has been carried out in the past few years [3–5]. These studies have revealed that the emissions of the first positive (1^+) and first negative (1^-) systems of nitrogen, corresponding respectively to the emissions associated with the transitions $N_2(B\,^3\Pi_g \rightarrow A\,^3\Sigma_u^+)$ and $N_2^+(B\,^2\Sigma_u^+ \rightarrow X\,^2\Sigma_g^+)$, increase in the afterglow after a dark zone positioned at the end of the discharge. The detected enhancement of the populations of the radiative states $N_2(B\,^3\Pi_g)$ and $N_2^+(B\,^2\Sigma_u^+)$ in the post-discharge motivated the quest for a similar behaviour in other species. This was recently achieved in [6], where the concentration of the metastable state $N_2(A\,^3\Sigma_u^+)$ and the electron density n_e in the afterglow were shown to have the same profile as the radiative states, that is they reach a minimum at the dark zone followed by a significant raise downstream. The aim of this paper is to give an insight in the understanding of the origin of such an intriguing behaviour exhibited by the nitrogen afterglow.

The emission of the 1^- system of nitrogen gives the first clue to solve this puzzle. In effect, it is well known that the excited ionic state $N_2^+(B\,^2\Sigma_u^+)$ is essentially populated via the near-resonant energy-exchange reaction [7, 8]

$$N_2(X\,^1\Sigma_g^+, v \geqslant 12) + N_2^+(X\,^2\Sigma_g^+) \longrightarrow N_2(X\,^1\Sigma_g^+, v') + N_2^+(B\,^2\Sigma_u^+), \quad (1)$$

so that ground-state ions $N_2^+(X\,^2\Sigma_g^+)$ must be created in the afterglow. On the other hand, N_2^+ ions (as well as N_4^+) can be created in the afterglow by collisions between the metastable states $N_2(A\,^3\Sigma_u^+)$ and $N_2(a'\,^1\Sigma_u^-)$, according to the Penning ionization reactions [9, 10]

$$N_2(A\,^3\Sigma_u^+) + N_2(a'\,^1\Sigma_u^-) \longrightarrow N_2(X\,^1\Sigma_g^+) + N_2^+(X\,^2\Sigma_g^+) + e \quad (2)$$

and

$$N_2(a'\,^1\Sigma_u^-) + N_2(a'\,^1\Sigma_u^-) \longrightarrow N_2(X\,^1\Sigma_g^+) + N_2^+(X\,^2\Sigma_g^+) + e. \quad (3)$$

These ionization mechanisms are the dominant channels for ionization even in a stationary N_2 discharge, in which electron impact ionization also takes place [11]. Therefore, a first conclusion is that both $N_2(A\,^3\Sigma_u^+)$ and $N_2(a'\,^1\Sigma_u^-)$ states need to be produced in the post-discharge. The possibility that they are created in the discharge and transported downstream to the afterglow is excluded by the existence of the dark zone before the raising of the 1^- emission. The problem is then reduced to explain the formation of the metastable species $N_2(A\,^3\Sigma_u^+)$

and $N_2(a'\,^1\Sigma_u^-)$ in the post-discharge. Once this is achieved, we can in principle explain not only the emission of the first negative system, but also the emission of the first positive system and the profile found for n_e. If $N_2(A\,^3\Sigma_u^+)$ is created in the post-discharge $N_2(B\,^3\Pi_g)$ is produced as well, as a result of the strong coupling existing between both states [11, 12], essentially via reaction

$$N_2(A\,^3\Sigma_u^+) + N_2(X\,^1\Sigma_g^+, 5 \leqslant v \leqslant 14) \longrightarrow N_2(X\,^1\Sigma_g^+, v = 0) + N_2(B\,^3\Pi_g). \quad (4)$$

This hypothesis was confirmed by De Benedictis and co-workers in [13], where the analysis of the vibrational distribution of the $N_2(B\,^3\Pi_g)$ state allowed to establish reaction (4) as the primary source of $N_2(B\,^3\Pi_g)$ in N_2 post-discharges. In what concerns the electron density, electrons are created through reactions (2) and (3) and will therefore follow, in principle, the same profile of the metastable states $N_2(A\,^3\Sigma_u^+)$ and $N_2(a'\,^1\Sigma_u^-)$.

The second important step in the interpretation of the behaviour of the different species in the nitrogen afterglow is the demonstration that only vibrationally excited molecules $N_2(X\,^1\Sigma_g^+, v)$, in levels as high as $v \gtrsim 35$, can be responsible for the appearance of the maxima in the concentrations localized downstream from the discharge after a dark zone. This was done in [14], where several mechanisms leading to the formation of electronic states have been investigated. The basic idea is that the very high vibrational levels of ground-state N_2 molecules, not significantly populated under discharge conditions due to the conjoint interplay of electron–vibration (e–V) and vibration–translation (V–T) collisions with N_2 molecules and N atoms [15], are strongly populated in the afterglow. This is the result of a pumping-up effect in the vibrational ladder due to near-resonant vibration–vibration (V–V) energy-exchanges, originating from of the anharmonicity of the potential-energy curve of $N_2(X\,^1\Sigma_g^+)$. As the e–V collisons cease to be effective, the action of V–T and V–V processes leads to a deactivation of the lower vth levels and a pumping of vibrational quanta into the higher ones [16].

In this work, we present a theoretical analysis that extends our previous results for the relaxation of heavy-particles in the nitrogen afterglow [14], by improving the description of the reactions involving highly excited vibrational levels of $N_2(X\,^1\Sigma_g^+)$. Here, we further include the kinetics of the atomic metastable states $N(^2D)$ and $N(^2P)$, not considered before, in the same way as in [17]. The inclusion in the model of the metastable atom kinetics is important to obtain a slow decay of $N_2(A\,^3\Sigma_u^+)$ at the beginning of the afterglow, due the recycling of metastables through reaction

$$N_2(X\,^1\Sigma_g^+, v \geqslant 10) + N(^2P) \longrightarrow N_2(A\,^3\Sigma_u^+) + N(^4S), \quad (5)$$

as was first noted in [6].

In what concerns the kinetics of electrons in the post-discharge, the relaxation of the electron energy distribution function (EEDF) in the afterglow was theoretically investigated in [18] by solving the time-dependent electron Boltzmann equation. In that paper it was shown that slow electrons remain for quite long times in the afterglow, until the transition from ambipolar to free diffusion regimes occurs. In the present work we have additionally considered in the Boltzmann equation the creation of new electrons through the Penning ionization reactions (2) and (3). When these reactions are taken into account in the model, the enhancement of the electron density in the post-discharge as it is experimentally observed is also well described. This corresponds to a first step in the achievement of a self-consistent solution coupling the electron and heavy-particle kinetics in the nitrogen afterglow.

The system under analysis is the nitrogen afterglow created by a discharge operating at frequency $\omega/2\pi = 433\,\text{MHz}$, pressure $p = 3.3\,\text{Torr}$, in a Pyrex tube of inner radius $R = 1.9\,\text{cm}$. The electron density at the beginning of the post-discharge is estimated to be $n_e(0) = 3\times10^{10}\,\text{cm}^{-3}$ [6].

The organization of this paper is as follows. In section 2, we describe the theoretical model used to study both the metastable and the electron kinetics in the nitrogen afterglow. Section 3 contains the results of the present investigation with the corresponding discussion, in which the theoretical calculations are compared with experimental data from [4, 6]. Finally, in section 4, we summarize the main conclusions.

2. Kinetic model

In this section, we describe the kinetic model developed to study a N_2 microwave afterglow. Our research must start with a detailed analysis of the discharge, since it is the discharge that establishes the conditions for the post-discharge. Once the solutions at the end of the discharge are known, they can be used as initial conditions in the set of equations describing the time-evolution of the different concentrations in the afterglow. Our approach provides a self-consistent formulation of the complex kinetics involved in nitrogen discharges and post-discharges, whose solution brings an important insight into the basic phenomena occurring in such a system.

2.1. Discharge

The kinetic models for nitrogen discharges under DC or HF fields, in which the electron and heavy-particle kinetics are coupled in a self-consistent way, have been described in [11,12,17]. The reader should refer to these papers for details, but a brief outline is given below.

Essentially, the EEDF is calculated by solving the homogeneous Boltzmann equation, using the two-term expansion in spherical harmonics. For the case of a microwave discharge we assume the effective field approximation [19], under which the angular field frequency ω is assumed sufficiently high so that the EEDF is nearly stationary. The effects produced by e–e Coulomb collisions are taken into account following the same procedure as in [20]. The electron Boltzmann equation is then coupled to a system of rate balance equations for the most important neutral and charged particles, such as the vibrationally excited molecules $N_2(X\,^1\Sigma_g^+, v)$, electronic states $N_2(A\,^3\Sigma_u^+$, $B\,^3\Pi_g$, $C\,^3\Pi_u$, $a'\,^1\Sigma_u^-$, $a\,^1\Pi_g$, $w\,^1\Delta_u$, $a''\,^1\Sigma_g^+)$, $N(^4S, ^2D, ^2P)$ atoms and N_2^+ and N_4^+ ions. The kinetic scheme for the discharge is the same as described in [11, 17], with the exception of the reaction for dissociation

$$N_2(X, v > 13) + N_2(A) \longrightarrow N_2(X) + N_2(B, v' \geqslant 13) \longrightarrow N_2(X) + N + N, \quad (6)$$

which was included here to compensate for a lack of production of $N(^4S)$ atoms and a larger amount of $N_2(A)$, predicted from the model in comparison with the measurements from [6]. We note that the need for an extra source of dissociation in N_2 discharges was recently pointed out in [21, 22]. Reaction $N_2(A) + N_2(A) \rightarrow N_2(X) + 2N$ was proposed in [21], while $2N_2(X, v > 10) \rightarrow N_2 + 2N$ was suggested in [22]. Here, we have considered reaction (6), as stated in [23], since the excitation of the non-predissociative v' levels of $N_2(B)$ is known to be very efficient through the reaction $N_2(X, v \geqslant 5) + N_2(A) \rightarrow N_2(B, v') + N_2(X)$ [24]. At the present stage it is not clear which mechanisms may constitute the additional channel that compensates for the lack of dissociation.

The reduced electric field sustaining the discharge is calculated using the requirement that under steady-state conditions the total rate for ionization must compensate exactly the rate of loss of electrons. The total rate of ionization includes electron impact on ground-state $N_2(X\,^1\Sigma_g^+)$ and metastable $N_2(A\,^3\Sigma_u^+)$ and $N_2(a'\,^1\Sigma_u^-)$ states, as well as reactions of Penning ionization between two metastables, $N_2(A) + N_2(a')$ and $N_2(a') + N_2(a')$ [11]. The quasi-neutrality condition imposes an additional constraint to the problem, ensuring that the ionic concentrations may be decoupled.

The input parameters of the discharge model are the common operating parameters, namely gas pressure, electron density, field frequency and tube radius. The gas temperature can be included in the system of equations, as it was done in [12,25], but here we will use it as an input parameter as well. The consideration of the electron density as an input parameter may seem odd at first sight. However, in the modelling of a microwave discharge it is equivalent to using either the power delivered to the discharge or the electron density at the position of the launcher. The electron density is a better input parameter in a model of this type, since it is difficult to estimate how much power will be absorbed by the launcher. A second remark is that the discharge presents in general an axial structure. For the case of a plasma produced by a surface wave, this structure was described in [25, 26]. Nevertheless, if we are interested in the discharge only as the source of the afterglow, we do not need to know the details of the axial structure. Since for the conditions of this study there is a local equilibrium between the different kinetics, the axial transport can be neglected [25], so that only the electron density close to the discharge end is of interest for this study. This value of the electron density can be estimated from the wave-dispersion characteristics, and it is the one used as input parameter in our model.

2.2. Metastable kinetics in the afterglow

The time-evolution of the concentrations of the different species in the post-discharge is analysed by considering the relaxation of a set of coupled kinetic master equations. The present investigation neglects processes involving electron impact in the afterglow. As will be shown, electron collisions are not absolutly vanishing, but they are not responsible for the appearance of the observed maxima in the afterglow, which are the phenomena under investigation in this paper. Therefore, the neglect of electron impact processes in the relaxation of the heavy-particles is justified within the purposes of the present study.

The set of reactions taken into account is based on the scheme described in [8, 11, 17], and it additionally includes a few new reactions. As was shown in [14], the enhancement of the concentrations of different species in a nitrogen post-discharge can only be explained by considering processes involving highly excited vibrational levels of $N_2(X\,^1\Sigma_g^+, v)$. Thus, we added to the system presented in [8, 17] the reactions for formation of $N_2(A\,^3\Sigma_u^+)$ and $N_2(a'\,^1\Sigma_u^-)$ states as a result of collisions between vibrationally excited molecules $N_2(X\,^1\Sigma_g^+, v)$ and long-lived ground-state $N(^4S)$ atoms, as follows:

$$N_2(X\,^1\Sigma_g^+, v \geqslant 39) + N(^4S) \longrightarrow N_2(A\,^3\Sigma_u^+) + N(^2D), \qquad (7)$$

$$N_2(X\,^1\Sigma_g^+, v \geqslant 38) + N(^4S) \longrightarrow N_2(a'\,^1\Sigma_u^-) + N(^4S). \qquad (8)$$

These reactions are allowed by spin conservation but the corresponding rate coefficients are unknown. Here, we will consider $k = 10^{-11}\,\mathrm{cm^3\,s^{-1}}$ for reaction (7) and $k = 10^{-12}\,\mathrm{cm^3\,s^{-1}}$ for reaction (8), which has been shown to be a suitable combination of these rate coefficients. The sensitivity of the results to the choice of the coefficients has been analysed in a preliminary work [27], whereas a detailed study will be presented in a forthcoming publication.

2.3. Electron kinetics in the afterglow

The study of the relaxation of the EEDF closely follows the formulation presented in [18]. The time-dependent Boltzmann equation is solved in the post-discharge, using the stationary EEDF obtained in the discharge as initial condition. In the post-discharge we assume zero electric field and we take into account a continuous transition from ambipolar to free diffusion regimes, resulting from the diminution of the space-charge field effects. The final form of the time-dependent Boltzmann equation was detailed in [18], in the case of the inclusion of elastic, inelastic, superelastic and electron–electron collisions, as well as of the terms accounting for the electron-loss processes associated with dissociative electron–ion recombination and electron diffusion under the space-charge field. Here, we consider as well the terms for creation of electrons by Penning ionization via reactions (2) and (3). If these reactions proceed with rate coefficients k_1 and k_2, respectively, in $\mathrm{cm^3\,s^{-1}}$ and create new electrons with energies u_1 and u_2, the electron creation processes correspond to the addition, on the right-hand side of equation (22) from [18], of a term of the form

$$\frac{1}{\sqrt{u}}\langle\nu_{\mathrm{ion}}\rangle n_{\mathrm{e}}, \qquad (9)$$

where $\langle\nu_{\mathrm{ion}}\rangle$ is a mean frequency for ionization associated with the Penning mechanism, defined per electron,

$$\langle\nu_{\mathrm{ion}}\rangle = \frac{[N_2(A)][N_2(a')]}{n_{\mathrm{e}}}k_1\delta(u_1) + \frac{[N_2(a')][N_2(a')]}{n_{\mathrm{e}}}k_2\delta(u_2). \qquad (10)$$

In this expression, $[N_2(A)]$ and $[N_2(a')]$ are functions of the afterglow time and denote the concentrations of the species $N_2(A\,^3\Sigma_u^+)$ and $N_2(a'\,^1\Sigma_u^-)$ at each instant, which are obtained by solving the system of rate balance equations for the heavy-particles already described. The δ functions obey the usual normalization condition $\int_0^\infty \delta(u)\,\mathrm{d}u = 1$.

We have also included in the Boltzmann equation the ionization reactions

$$N_2(X\,^1\Sigma_g^+, v \geqslant 30) + N_2(a'\,^1\Sigma_u^-) \longrightarrow N_2(X\,^1\Sigma_g^+) + N_2^+(X\,^2\Sigma_g^+) + e \quad (11)$$

and

$$N_2(X\,^1\Sigma_g^+, v \geqslant 36) + N_2(B\,^3\Pi_g) \longrightarrow N_2(X\,^1\Sigma_g^+) + N_2^+(X\,^2\Sigma_g^+) + e, \quad (12)$$

as suggested in [28]. However, under the present conditions these two reactions give only a minor contribution to the calculated electron densities.

The procedure described above corresponds to an effective coupling between the heavy-particle and the electron kinetics in the post-discharge. However, it does not determine a full self-consistent solution to the problem. Such a solution would also require the inclusion of electron processes in the master equations for the heavy-particles, as well as an iterative procedure between heavy-particle and electron kinetics. Nevertheless, the present formulation already predicts very fairly the main trends for all the species involved in the system. The improvement introduced by using an iterative procedure should be noticeable specially for the early instants of the afterglow. Another point of inconsistency is that we assume, in the solution to the electron Boltzmann equation, that the population of the first ten vibrational levels of $N_2(X\,^1\Sigma_g^+)$ molecules do not vary significantly in the post-discharge. For the present conditions this can be considered as a good approximation up to afterglow times of the order of 10^{-3}–10^{-2} s, but it will start to fail for longer times, as shown below.

3. Results and discussion

The calculations were carried out for the experimental conditions of [4, 6]. In particular, we consider a discharge operating at $\omega/2\pi = 433$ MHz, $p = 3.3$ Torr, inner tube radius $R = 1.9$ cm and initial electron density $n_e(0) = 3 \times 10^{10}$ cm^{-3}. The gas temperature in the discharge was assumed to be $T_g = 1000$ K, whereas the experimental values reported in [6] for T_g were considered in the afterglow. For this set of parameters, the calculated discharge parameters are $E_e/N = 4.6 \times 10^{-16}$ V cm^2 for the effective sustaining electric field [29] and $T_v = 6124$ K for the characteristic vibrational temperature of the Treanor-like distribution that best fits the calculated vibrational distribution function (VDF) of $N_2(X\,^1\Sigma_g^+)$ molecules in the lowest four levels.

In order to illustrate the V–V pumping-up effect, figure 1 shows the calculated VDFs at different instants in the post-discharge: $t = 0$ (A), 10^{-4} s (B), 10^{-3} s (C), 10^{-2} s (D) and 10^{-1} s (E). The tail of the VDF passes through a pronounced maximum for times of the order of 10^{-3}–10^{-2} s. As was already stated, this is a consequence of the near-resonant V–V exchanges. The anhamonicity of the oscillator implies that the energy difference between neighbouring vibrational levels decreases from the bottom to the top of the vibrational ladder. Therefore, the forward and backward reactions

$$N_2(X\,^1\Sigma_g^+, v) + N_2(X\,^1\Sigma_g^+, w) \leftrightharpoons N_2(X\,^1\Sigma_g^+, v-1) + N_2(X\,^1\Sigma_g^+, w+1), \quad (13)$$

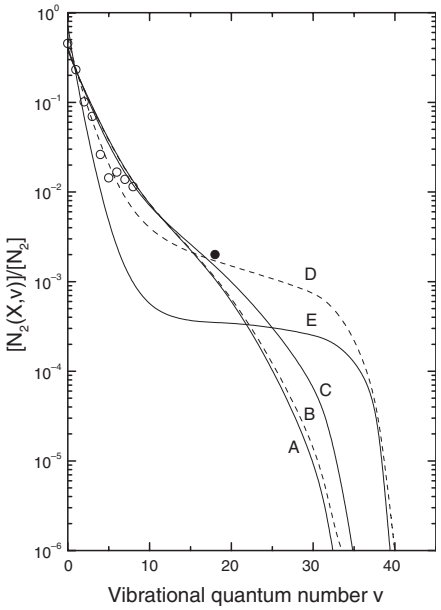

Figure 1. VDF of $N_2(X\,^1\Sigma_g^+)$ molecules as a function of the afterglow time at $t = 0$ (A), 10^{-4} s (B), 10^{-3} s (C), 10^{-2} s (D) and 10^{-1} s (E). The experimental points correspond to the measurements reported in [5] at $t \sim 1.5 \times 10^{-2}$ s (○) and in [30] for a dc discharge at $p = 2.3$ Torr and $I = 100$ mA (●).

with $v < w$, have a larger rate coefficient for collisions that lead to a gain of vibrational quanta for the higher wth levels and loss of quanta for the lower vth ones. Figure 1 depicts as well a couple of measurements available in the literature: the Raman scattering measurements at the position of the maximum of the emission intensities, corresponding to $t \sim 1.5 \times 10^{-2}$ s, from [5] (open circles); and the cavity ringdown spectroscopy measurement of the population of level $v = 18$ in a DC discharge at $p = 2.3$ Torr and $I = 100$ mA from [30] (black circle). Although the available measurements cannot confirm or refute the behaviour of the very high levels of the calculated VDFs, the agreement with the experiments for the measured vibrational levels is quite remarkable.

Whereas the levels $v \gtrsim 35$ pass through significant maxima at times close to 10^{-2} s, this effect is significantly smaller for lower levels, of say $v \sim 20$. Accordingly, these low levels cannot be involved in the explanation of the appearance of narrow maxima for the populations of the different species arising after a dark zone. This can be reinforced by inspection of figure 2, where we plot the population of some vibrational levels normalized to their concentration at the beginning of the post-discharge. It can be clearly confirmed that only the highest vibrational levels of $N_2(X\,^1\Sigma_g^+)$, typically larger than $v \sim 35$, show the correct profile in order to explain the behaviour found in the nitrogen afterglow.

Figures 1 and 2 confirm the validity of the assumption of a near constant population in levels $0 \leqslant v \leqslant 10$ up to times of 10^{-3} s that we have made in the solution of the time-dependent electron Boltzmann equation (see above). As shown here, this hypothesis is no longer valid for $t \gtrsim 10^{-2}$ s. That being so, the results presented in this work for the electron kinetics at the far remote afterglow should be regarded as merely indicative.

At this point it is worth noting that the VDF calculated in the discharge ($t = 0$) is very distant from a Boltzmann

distribution, as can be seen from curve A in figure 1. In particular, even if the plateau formed at intermediate vth levels [31] is not very pronounced, all the levels $v \gtrsim 10$ of the actual VDF are overpopulated when compared with a Boltzmann distribution for the same vibrational temperature. Thus, any calculations for the afterglow that assume a Boltzmann VDF at $t = 0$, as it was done in [32], are likely to result in erroneous interpretations.

In figure 3, we show the comparison between the calculated and measured densities of ground-state $N(^4S)$ atoms. The measurements were taken from [33] and were obtained by two-photon laser-induced fluorescence. The agreement between predicted and measured values is quite satisfactory. It can be seen that the atomic concentration remains essentially constant along the afterglow until times of the order of 10^{-1} s. In this way, there are always $N(^4S)$ atoms available to participate in reactions (7) and (8), so that the source terms of $N_2(A\ ^3\Sigma_u^+)$ and $N_2(a'\ ^1\Sigma_u^-)$ states associated with these two reactions follow the profile of the vibrationally excited molecules $N_2(X\ ^1\Sigma_g^+, v \geqslant 38)$, presented in figure 2.

The existence of nitrogen atoms along all the post-discharge region has motivated the suggestion that a temperature effect in the three-body atomic recombination could be in the origin of the observed peaks for the concentrations of different species [6]. This explanation was ruled out in [27], where this mechanism was tested and analysed in detail.

Figures 4 and 5 show the relative populations of the radiative states $N_2(B\ ^3\Pi_g)$ and $N_2^+(B\ ^2\Sigma_u^+)$, respectively, obtained from the present model (full curves) and measured in [4, 6]. Since the emission measurements are relative, the peak values were normalized to be close to those calculated here. The behaviour of both emissions is well described by the present model. The main differences between measurements and calculations are most certainly due to the uncertainties in the rate coefficients for V–T deactivation of $N_2(X\ ^1\Sigma_g^+, v)$ by $N(^4S)$ atoms. As has been already said, a detailed study of the effect of the rate coefficients of reactions (7) and (8) will be presented elsewhere. Nevertheless, figures 4 and 5 show as well the results obtained when these rate coefficients are both zero (dashed curves), strikingly confirming the complete absence of a rising of the emissions in this case.

The emission of the $N_2(C\ ^3\Pi_u)$ state is also an important emission in nitrogen post-discharges but it was not analysed

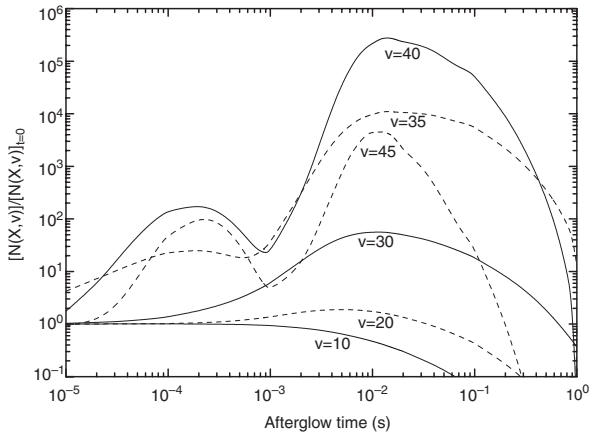

Figure 2. Time-evolution of the population of some particular vibrational levels, $[N_2(X\ ^1\Sigma_g^+)]$, normalized to their population at $t = 0$, $[N_2(X\ ^1\Sigma_g^+)]_{(t=0)}$.

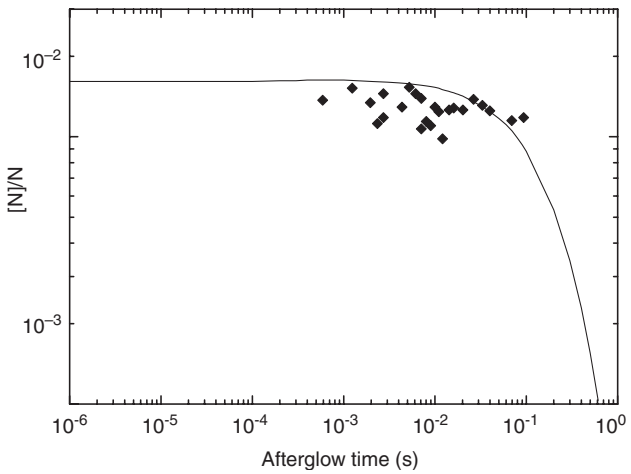

Figure 3. Comparison between our model predictions and the measured data [33] for $[N(^4S)]/N$, as a function of afterglow time.

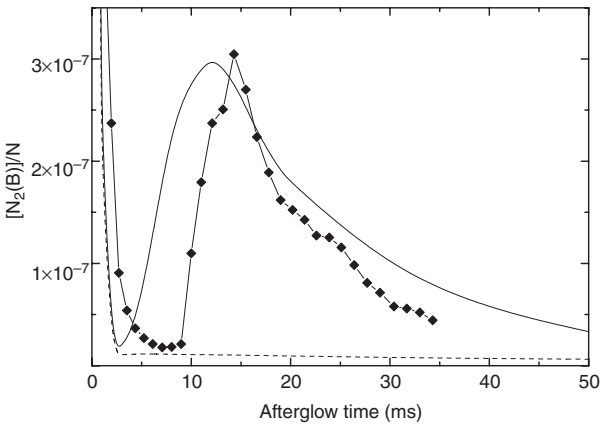

Figure 4. Comparison between our model predictions (——) and the measured data [6] (–♦–) for $[N_2(B\ ^3\Pi_g)]/N$, as a function of afterglow time. The dashed curve corresponds to the model predictions when reactions (7) and (8) are neglected.

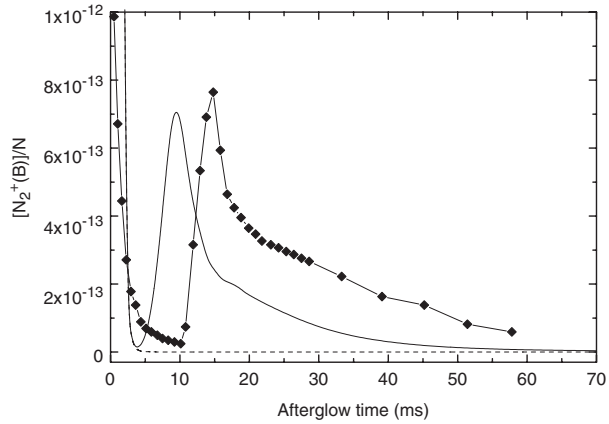

Figure 5. Comparison between our model predictions (——) and the measured data [4] (–♦–) for $[N_2^+(B\ ^2\Sigma_u^+)]/N$, as a function of afterglow time. The dashed curve corresponds to the model predictions when reactions (7) and (8) are neglected.

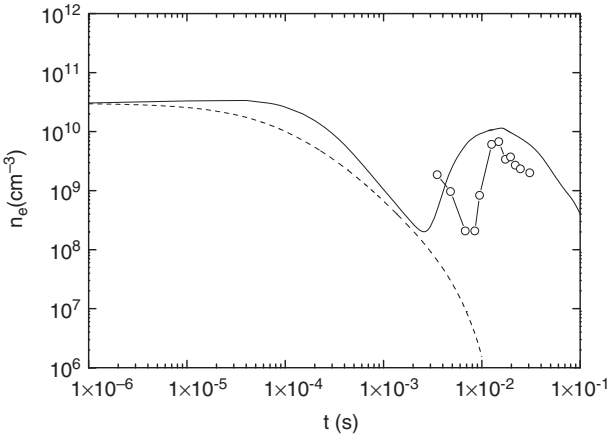

Figure 6. Comparison between our model predictions and the measured data [6] for the electron density n_e, as a function of afterglow time, when the reactions (2), (3), (11) and (12) for Penning ionization are included (——) and neglected (· · · · · ·).

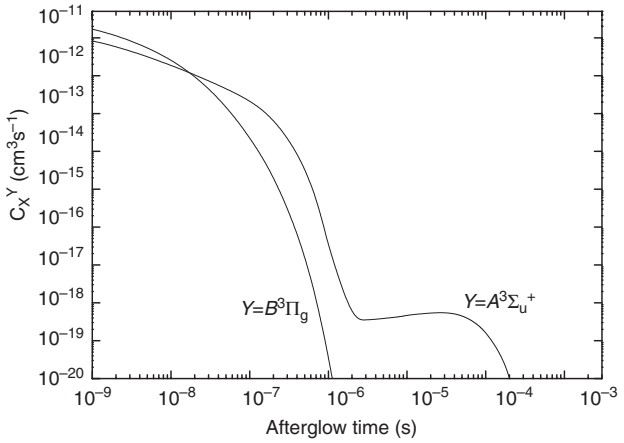

Figure 7. Temporal evolution of the electron rate coefficients for excitation of $N_2(A\ ^3\Sigma_u^+)$ and $N_2(B\ ^3\Pi_g)$ states from the electronic ground-state $N_2(X\ ^1\Sigma_g^+)$.

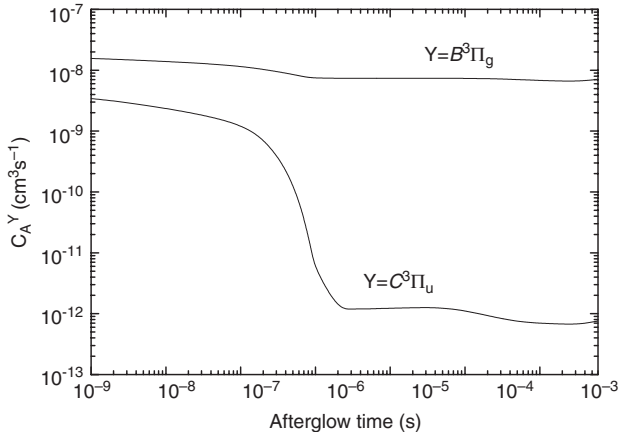

Figure 8. Temporal evolution of the electron rate coefficients for stepwise excitation of $N_2(B\ ^3\Pi_g)$ and $N_2(C\ ^3\Pi_u)$ states from $N_2(A\ ^3\Sigma_u^+)$.

here due to the lack of experimental data for comparison. For the sake of curiosity, it can be said that according to the present calculations this emission also passes through a maximum after the dark zone, as a result of the pooling reaction $N_2(A) + N_2(A) \rightarrow N_2(C) + N_2(X)$ and of collisions between vibrationally excited molecules in levels $N_2(X\ ^1\Sigma_g^+, v \geqslant 20)$ and $N_2(A\ ^3\Sigma_u^+)$ metastables.

Figure 6 presents the electron density in the afterglow calculated by solving the time-dependent Boltzmann equation, together with the experimental values reported in [6]. The full and dotted curves correspond, respectively, to the inclusion and neglect in the model of the ionization reactions involving heavy-species (2), (3), (11) and (12). In the conditions of this study the latter two reactions do not contribute appreciably to the total rate for production of secondary electrons. When we include the reactions of Penning ionization the predicted profile for n_e is in good agreement with the measured one. That being so, we can conclude that reactions (7) and (8) are also in the origin of the maximum observed for the electron density, since they create the metastable species that participate in the ionization of the gas. We note that even in the absence of creation of new electrons, the electron density remains almost constant in the afterglow for quite long times ($t \sim 10^{-3}$–10^{-2} s). This is a consequence of the large characteristic times for electron ambipolar diffusion, as was pointed out in [18], and it is in agreement with the measurements done in [34], where the variation of the effective diffusion coefficient was derived from breakdown time delay data. Very recently this effect was also detected in a corona discharge [35].

Since we have electrons in the post-discharge, the question arises on whether or not they can be involved in electron-impact excitation processes. The existence of electron processes influencing the heavy-particle kinetics was first pointed out in [36] and subsequently in [13, 37]. The theoretical analysis presented in [18] has demonstrated that although the high energy tail of the EEDF is rapidly depleted, the rate coefficients for some low-energy threshold processes, such as the stepwise excitation of $N_2(B\ ^3\Pi_g)$ and $N_2(C\ ^3\Pi_u)$ states from $N_2(A\ ^3\Sigma_u^+)$, are much slower modified. In order to illustrate this effect for the conditions of this study, figure 7 shows the rate coefficients for electron impact excitation of $N_2(A\ ^3\Sigma_u^+)$ and $N_2(B\ ^3\Pi_g)$ states from the ground-state $N_2(X\ ^1\Sigma_g^+)$, while in figure 8 we plot the rate coefficients for stepwise excitation of $N_2(B\ ^3\Pi_g)$ and $N_2(C\ ^3\Pi_u)$ from $N_2(A\ ^3\Sigma_u^+)$.

Inspection of figure 7 reveals that the electron rate coefficients for excitation of $N_2(A\ ^3\Sigma_u^+)$ and $N_2(B\ ^3\Pi_g)$ states from $N_2(X\ ^1\Sigma_g^+)$ are rapidly reduced in consequence of the depletion of the high-energy tail of the EEDF at the first instants of the afterglow [18]. For an afterglow time as small as $t \sim 10^{-7}$ s the excitation coefficient of $N_2(B\ ^3\Pi_g)$ state has already decreased by about three orders of magnitude, while at $t \sim 10^{-6}$ s the excitation coefficient of $N_2(A\ ^3\Sigma_u^+)$ state, which has an energy threshold of 6.2 eV, has dropped seven orders of magnitude. This fast depopulation of the high-energy part of the EEDF is the result of electron inelastic collisions. On the other hand, for times greater than $t \sim 10^{-6}$ s there is a quasi-equilibrium between the EEDF and the VDF, through inelastic and superelastic collisions, and the changes in the EEDF become much slower. From figure 7 it is perfectly clear that electron impact excitation of electronic states from ground-state $N_2(X\ ^1\Sigma_g^+)$ molecules are negligible in a post-discharge.

Finally, in figure 8 we can observe that under the present conditions stepwise excitation of $N_2(B\,^3\Pi_g)$ and $N_2(C\,^3\Pi_u)$ states from $N_2(A\,^3\Sigma_u^+)$ remains significant at least up to $t \sim 10^{-2}$ s. Accordingly, these processes can play a non-negligible role in the post-discharge.

4. Conclusions

In this work, we have shown that the peculiar behaviour observed in the nitrogen afterglow of a flowing discharge, namely the existence of narrow maxima in the concentrations of several species occurring after a dark zone, can be well explained by assuming the creation of the electronic metastable species $N_2(A\,^3\Sigma_u^+)$ and $N_2(a'\,^1\Sigma_u^-)$ in the afterglow. Furthermore, it has been demonstrated that the formation of these two states in the afterglow can only occur in reactions involving collisions of highly excited vibrational levels of $N_2(X\,^1\Sigma_g^+)$, in levels as high as $v \sim 35$. This is a result of the near-resonant V–V exchanges, which produce a pumping-up effect into the vibrational ladder.

A very probable mechanism for production of metastables $N_2(A\,^3\Sigma_u^+)$ and $N_2(a'\,^1\Sigma_u^-)$ is via reactions (7) and (8), reproduced below:

$$N_2(X\,^1\Sigma_g^+, v \geqslant 39) + N(^4S) \longrightarrow N_2(A\,^3\Sigma_u^+) + N(^2D)$$

and

$$N_2(X\,^1\Sigma_g^+, v \geqslant 38) + N(^4S) \longrightarrow N_2(a'\,^1\Sigma_u^-) + N(^4S).$$

Once the metastable states are created in the post-discharge, $N_2(B\,^3\Pi_g)$ is formed through reaction (4),

$$N_2(A\,^3\Sigma_u^+) + N_2(X\,^1\Sigma_g^+, 5 \leqslant v \leqslant 14) \longrightarrow N_2(X\,^1\Sigma_g^+, v = 0) + N_2(B\,^3\Pi_g),$$

whereas N_2^+ ions and electrons are formed by the Penning ionization mechanisms (2) and (3),

$$N_2(A\,^3\Sigma_u^+) + N_2(a'\,^1\Sigma_u^-) \longrightarrow N_2(X\,^1\Sigma_g^+) + N_2^+(X\,^2\Sigma_g^+) + e$$

and

$$N_2(a'\,^1\Sigma_u^-) + N_2(a'\,^1\Sigma_u^-) \longrightarrow N_2(X\,^1\Sigma_g^+) + N_2^+(X\,^2\Sigma_g^+) + e.$$

The radiative species $N_2^+(B\,^2\Sigma_u^+)$ is then formed by reaction (1),

$$N_2(X\,^1\Sigma_g^+, v \geqslant 12) + N_2^+(X\,^2\Sigma_g^+) \longrightarrow N_2(X\,^1\Sigma_g^+, v') + N_2^+(B\,^2\Sigma_u^+).$$

This set of reactions provides a good interpretation for the available experimental data in the nitrogen afterglow.

In what concerns the electron kinetics, all the conclusions obtained in [18] were confirmed for the conditions of the present study. The EEDF is quickly modified at the first instants of the afterglow. The direct excitation of the electronic states by electron impact is no longer effective for times as short as $t \sim 10^{-7}$ s. However, the electron density remains important up to much longer times, which may even reach $t \sim 10^{-1}$ s. This is the result of the large characteristic times for ambipolar diffusion, together with the efficient creation of new electrons by reactions (2) and (3) for Penning ionization. These two reactions also explain the observed maximum for the electron density in the post-discharge region, and illustrate the important coupling between electron and metastable kinetics in the nitrogen afterglow. Since slow electrons remain for a long time, some low-threshold electron excitation processes can play a non-negligible role. This is the case of stepwise excitation of $N_2(B\,^3\Pi_g)$ and $N_2(C\,^3\Pi_u)$ states from $N_2(A\,^3\Sigma_u^+)$.

Although at the present stage we have already included the effects of Penning ionization in the electron Boltzmann equation, a full self-consistent solution to the study of nitrogen post-discharges has not been achieved here. Future work should proceed in this direction, concentrating on three main points. First, the inclusion of electron impact processes in the kinetics of heavy-particles. Second, the consideration of a time-dependent VDF for the lower levels of $N_2(X\,^1\Sigma_g^+, v)$ in the study of the electron kinetics. Finally, the investigation of the effect of superelastic collisions of electrons with electronically excited N_2 states on the EEDF and on the concentrations for these species. These refinements will certainly increase our knowledge of the elementary phenomena occurring in the nitrogen afterglow. Nevertheless, although the inclusion of these effects may lead to some changes in the quantitative results, our preliminary results indicate it will not alter the basic viewpoint of the pink afterglow phenomena presented in this paper.

Acknowledgments

The authors are indebted to Dr N Sadeghi and Dr P Supiot for fruitful discussions. The authors also wish to thank Dr A Salabas for his help with some numerical details.

References

[1] Ricard A, Oseguera-Pena J E, Falk L, Michel H and Gantois M 1990 Active species in microwave postdischarge for steel-surface nitriding *IEEE Trans. Plasma Sci.* **18** 940–4

[2] Boisse-Laport C, Normand-Chave C and Marec J 1997 A microwave plasma source of neutral nitrogen atoms *Plasma Sources Sci. Technol.* **6** 70–7

[3] Supiot P, Dessaux O and Goudmand P 1995 Spectroscopic analysis of the nitrogen short-lived afterglow induced at 433 mhz *J. Phys. D: Appl. Phys.* **28** 1826–39

[4] Blois D, Supiot P, Barj M, Chapput A, Foissac C, Dessaux O and Goudmand P 1998 The microwave source's influence on the vibrational energy carried by $N_2(X\,^1\Sigma_g^+)$ in a nitrogen afterglow *J. Phys. D: Appl. Phys.* **31** 2521–31

[5] Supiot P, Blois D, De Benedictis S, Dilecce G, Barj M, Chapput A, Dessaux O and Goudmand P 1999 Excitation of $N_2(B\,^3\Pi_g)$ in the nitrogen short-lived afterglow *J. Phys. D: Appl. Phys.* **32** 1887–93

[6] Sadeghi N, Foissac C and Supiot P 2001 Kinetics of $N_2(A\,^3\Sigma_u^+)$ molecules and ionization mechanisms in the afterglow of a flowing N_2 microwave discharge *J. Phys. D: Appl. Phys.* **34** 1779–88

[7] Gordiets B F, Ferreira C M, Guerra V L, Loureiro J M A H, Nahorny J, Pagnon D, Touzeau M and Vialle M 1995 Kinetic model of a low-pressure N_2–O_2 flowing glow discharge *IEEE Trans. Plasma. Sci.* **23** 750–67

[8] Sá P A and Loureiro J 1997 A time-dependent analysis of the nitrogen afterglow in N_2 and N_2–Ar microwave discharges *J. Phys. D: Appl. Phys.* **30** 2320–30

[9] Brunet H and Rocca-Serra J 1985 Model for a glow discharge in flowing nitrogen *J. Appl. Phys.* **57** 1574–81

[10] Berdyshev A V, Kochetov I V and Napartovich A P 1988 Ionization mechanism in a quasisteady glow discharge in pure nitrogen *Sov. J. Plasma Phys.* **14** 438–40

[11] Guerra V and Loureiro J 1997 Electron and heavy particle kinetics in a low pressure nitrogen glow discharge *Plasma Sources Sci. Technol.* **6** 361–72

[12] Guerra V, Sá P A and Loureiro J 2001 Role played bt the $N_2(A\,^3\Sigma_u^+)$ metastable in stationary N_2 and N_2–O_2 discharges *J. Phys. D: Appl. Phys.* **34** 1745–55

[13] De Benedictis S, Dilecce G and Simek M 1999 Excitation and decay of $N_2(B\,^3\Pi_g, v)$ states in a pulsed discharge: kinetics of electrons and long-lived species *J. Chem. Phys.* **110** 2947–62

[14] Loureiro J, Sá P A and Guerra V 2001 Role of long-lived $N_2(X\,^1\Sigma_g^+, v)$ molecules and $N_2(A\,^3\Sigma_u^+)$ and $N_2(a'\,^1\Sigma_u^-)$ states in the light emissions of a N_2 afterglow *J. Phys. D: Appl. Phys.* **34** 1769–78

[15] Guerra V and Loureiro J 1995 Non-equilibrium coupled kinetics in stationary N_2–O_2 discharges *J. Phys. D: Appl. Phys.* **28** 1903–18

[16] Cacciatore M, Capitelli M and Gorse C 1982 Non-equilibrium dissociation and ionization of nitrogen in electrical discharges: the role of electronic collisions from vibrationally excited molecules *Chem. Phys.* **66** 141–51

[17] Guerra V, Tatarova E and Ferreira C M 2003 Kinetics of metastable atoms and molecules in N_2 microwave discharges *Vacuum* **69** 171–6

[18] Guerra V, Sá P A and Loureiro J 2001 Relaxation of the electron energy distribution function in the afterglow of a N_2 microwave discharge including space-charge field effects *Phys. Rev.* E **63** 046404–1–13

[19] Ferreira C M and Loureiro J 1989 Electron excitation rates and transport parameters in high-frequency N_2 discharges *J. Phys. D: Appl. Phys.* **22** 76–82

[20] Sá P A, Loureiro J and Ferreira C M 1992 Effects of electron-electron collisions on the characteristics of DC and microwave discharges in argon at low pressures *J. Phys. D: Appl. Phys.* **25** 960–6

[21] Gordiets B F, Ferreira C M, Pinheiro M J and Ricard A 1998 Self-consistent kinetic model of low-pressure N_2–H_2 flowing discharges: I. Volume processes *Plasma Sources Sci. Technol.* **7** 363–78

[22] Brovikova I N and Galiaskarov E G 2001 Kinetic characteristics of production and loss of nitrogen atoms in N_2 plasma *High Temp.* **39** 809–14

[23] Slovetskii D I 1980 *Mechanisms of Chemical Reactions in Nonequilibrium Plasmas* (Moscow: Nauka)

[24] Piper L G 1989 The excitation of $N_2(B\,^3\Pi_g, v' = 1$–$12)$ in the reaction between $N_2(A\,^3\Sigma_u^+)$ and $N_2(X, v \geqslant 5)$ *J. Chem. Phys.* **91** 864–73

[25] Guerra V, Tatarova E, Dias F M and Ferreira C M 2002 On the self-consistent modeling of a traveling wave sustained nitrogen discharge *J. Appl. Phys.* **91** 2648–61

[26] Tatarova E, Dias F M, Ferreira C M and Ricard A 1999 On the axial structure of a nitrogen surface wave sustained discharge: theory and experiment *J. Appl. Phys.* **85** 49–62

[27] Sá P A, Guerra V, Loureiro J and Sadeghi N 2002 Self-consistent modelling of a flowing nitrogen microwave discharge for interpretation of afterglow data *16th European Conf. on Atomic and Molecular Physics of Ionized Gases—5th International Conf. on Reactive Plasmas Joint Meeting* vol 2, ed N Sadeghi and H Sugai *(Grenoble, France, 2002)* (European Physical Society) pp 91–2

[28] Dias F M, Supiot P, Guerra V, Dupret C, Popov T, Sá P A and Loureiro J 2001 Electron energy distribution function in the afterglow of a microwave discharge in flowing nitrogen *15th International Symp. on Plasma Chemistry (ISPC)* ed A Bouchoule *et al (Orléans, France, 2001)* pp 545–50

[29] Ferreira C M and Moisan M 1988 The similarity laws for the maintenance field and the absorbed power per electron in low-pressure surface wave produced plasmas and their extension to HF plasmas in general *Physica Scr.* **38** 382–99

[30] Macko P, Cunge G and Sadeghi N 2001 Density of $N_2(X\,^1\Sigma_g^+, v = 18)$ molecules in a dc glow discharge measured by cavity ringdown spectroscopy at 227 nm; validity domain of the technique *J. Phys. D: Appl. Phys.* **34** 1807–11

[31] Loureiro J and Ferreira C M 1986 Coupled electron energy and vibrational distribution functions in stationary N_2 discharges *J. Phys. D: Appl. Phys.* **19** 17–35

[32] Levaton J, Amorim J, Sousa A R, Franco D and Ricard A 2002 Kinetics of atoms, metastable, radiative and ionic species in the nitrogen pink afterglow *J. Phys. D: Appl. Phys.* **35** 689–98

[33] Mazouffre S, Engelm R, Vankan P, Schram D, Foissac C, Supiot P and Sadeghi N 2001 Density and temperature of N atoms in the afterglow of a microwave discharge measured by two-photon laser induced fluorescence technique *Plasma Sources Sci. Technol.* **10** 168–75

[34] Vidosav Lj Marković, Zoran Lj Petrović and Pejović M M 1997 Modelling of charged particle decay in nitrogen afterglow *Plasma Sources Sci. Technol.* **6** 240–6

[35] De Benedictis S 2002 Private communication

[36] De Benedictis S and Dilecce G 1995 Vibrational relaxation of $N_2(C, v)$ state in N_2 pulsed rf discharge: electron impact and pooling reactions *Chem. Phys.* **192** 149–62

[37] Cartry G, Magne L and Cernogora G 1999 Experimental study and modelling of a low-pressure N_2–O_2 time afterglow *J. Phys. D: Appl. Phys.* **32** 1894–907